Published in final edited form as:
J Mech Behav Biomed Mater. 2012 July ; 11: 123–131. doi:10.1016/j.jmbbm.2011.11.007.

A silk hydrogel-based delivery system of bone morphogenic protein for the treatment of large bone defects

Tamim Diab[a,*], **Eleanor M. Pritchard**[b,*], **Brent A. Uhrig**[a,c], **Joel D. Boerckel**[a,c], **David L. Kaplan**[b], and **Robert E. Guldberg**[a,c]

Tamim Diab: tdiab@gatech.edu; Eleanor M. Pritchard: eleanor.Pritchard@tufts.edu; Brent A. Uhrig: brent.uhrig@gatech.edu; Joel D. Boerckel: joel.boerckel@gatech.edu; David L. Kaplan: david.kaplan@tufts.edu; Robert E. Guldberg: robert.guldberg@me.gatech.edu

[a]Parker H. Petit Institute for Bioengineering and Bioscience, Georgia Institute of Technology, Atlanta, GA

[b]Department of Biomedical Engineering, Tufts University, Medford, MA

[c]George W. Woodruff School of Mechanical Engineering, Georgia Institute of Technology, Atlanta, GA

Abstract

The use of tissue grafting for the repair of large bone defects has numerous limitations including donor site morbidity and the risk of disease transmission. These limitations have prompted research efforts to investigate the effects of combining biomaterial scaffolds with biochemical cues to augment bone repair. The goal of this study was to use a critically-sized rat femoral segmental defect model to investigate the efficacy of a delivery system consisting of an electrospun polycaprolactone (PCL) nanofiber mesh tube with a silk fibroin hydrogel for local recombinant bone morphogenetic protein 2 (BMP-2) delivery. Bilateral 8 mm segmental femoral defects were formed in 13-week-old Sprague Dawley rats. Perforated electrospun PCL nanofiber mesh tubes were fitted into the adjacent native bone such that the lumen of the tubes contained the defect (Kolambkar et al., 2011b). Silk hydrogels with or without BMP-2 were injected into the defect. Bone regeneration was longitudinally assessed using 2D X-ray radiography and 3D microcomputed topography (μCT). Following sacrifice at 12 weeks after surgery, the extracted femurs were either subjected to biomechanical testing or assigned for histology. The results demonstrated that silk was an effective carrier for BMP-2. Compared to the delivery system without BMP-2, the delivery system that contained BMP-2 resulted in more bone formation ($p < 0.05$) at 4, 8, 12 weeks after surgery. Biomechanical properties were also significantly improved in the presence of BMP-2 ($p < 0.05$) and were comparable to age-matched intact femurs. Histological evaluation of the defect region indicated that the silk hydrogel have completely been degraded by the end of the study. Based on these results, we conclude that a BMP-2 delivery system consisting of an electrospun PCL nanofiber mesh tube with a silk hydrogel presents an effective strategy for functional repair of large bone defects.

Corresponding author: Robert E. Guldberg, Ph.D., Institute for Bioengineering and Biosciences, 315 Ferst Drive Georgia Institute of Technology, Atlanta, GA 30332-0363 USA tel: 404.894.6589 fax: 404.894.2291, robert.guldberg@me.gatech.edu, Phone: (404) 894-6589 Fax: (404) 385-1397.
*indicates equal contribution

Keywords

bone regeneration; silk; biomaterials; growth factor carrier

Introduction

The timely repair of critically sized bone defects/damage remains a major unmet clinical challenge. Bone grafts have been the principal treatment modalities for augmenting or accelerating bone regeneration, but suffer from significant drawbacks. Autologous grafts suffer from the disadvantages of limited material available for grafting, the need for a second graft-harvesting surgery, and donor site morbidity (Kirker-Head et al., 2007; Kolambkar et al., 2011b; Wang et al., 2006). Allografts and xenografts exhibit high failure rates and carry the risks of immune-mediated rejections and transmission of infection from donor to host (Kirker-Head et al., 2007; Kolambkar et al., 2011b). These limitations have prompted research efforts to investigate the effects of combining scaffolds with biochemical cues to augment bone repair.

A variety of scaffold technologies have been explored for bone tissue engineering. One of the more recent and promising scaffold technologies for the repair of critically sized long bone defects is based on placing an electrospun polycaprolactone (PCL) nanofiber mesh membrane (or tube) along the periosteal surface of the defect region (Boerckel et al., 2011; Kolambkar et al., 2011a; Kolambkar et al., 2011b). The main advantage of using a membrane compared to a 3D scaffold is that it will not impede cellular infiltration and bone formation in the defect region (Kolambkar et al., 2011b). Another important feature of using a membrane is that it will act as a barrier to separate the osseous and non-osseous regions (Kolambkar et al., 2011b).

Bone repair can also be enhanced through biochemical cues via the delivery of growth factors (Luginbuehl et al., 2004; Wang et al., 2006). Bone morphogenetic protein 2 (BMP-2) has sparked interest due to its ability to promote new bone formation (Bessa et al., 2010a; Bessa et al., 2010b; Chen et al., 2007). However, the practical administration of growth factors is associated with numerous challenges. Large doses of BMP-2 are required, making potential therapies expensive (Chen et al., 2007; Kolambkar et al., 2011b). Delivery of growth factors via systemic or direct injection is limited by slow tissue penetration, short half-lives, and rapid diffusion from the injection site (Chen et al., 2007). Frequent, clinically-impractical injections would be required to maintain high growth factor concentrations for long time frames (Chen et al., 2007). If delivery is not localized, BMP-2 can induce systemic side-effects, including the formation of ectopic bone and excessive inflammation in adjacent soft tissues (Carragee et al., 2011; Luginbuehl et al., 2004; Wang et al., 2009).

One option to improve the safety, efficacy, and feasibility of growth factor delivery is by incorporation into biomaterials. Local sustained delivery limits systemic exposure and increases the efficacy of a lower protein dose (Kolambkar et al., 2011b). Biomaterial carriers can also potentially increase growth factor lifetime and stability and exert control over release kinetics (Bessa et al., 2010a; Bessa et al., 2010b; Wang et al., 2009). The commercially-available delivery system based on rhBMP-2 solution applied to an absorbable collagen sponge (ACS) has significant limitations, including susceptibility of the collagen sponge carrier to premature resorption and compression (Suh et al., 2002), the use of high doses of rhBMP-2, and the need for bulking agent (grafting with the sponge alone results in a thin, structurally weak fusion and the need for high doses of rhBMP-2) (Glassman et al., 2007). Silk fibroin (a protein polymer isolated from the cocoons of the

domestic silkworm, *Bombyx mori*) possesses unique properties for bone tissue engineering. Silk possesses excellent biocompatibility (Leal-Egana and Scheibel, 2010; Meinel et al., 2005; Panilaitis et al., 2003; Seo et al., 2009), degrades to non-toxic products *in vivo* and the degradation time course of silk implants can be readily manipulated (Horan et al., 2005; Numata and Kaplan, 2010; Wang et al., 2008b). Silk can be processed entirely in aqueous systems without the use of harsh manufacturing conditions that can potentially deactivate the incorporated growth factor (Lawrence et al., 2008; Vepari and Kaplan, 2007). In particular, stable, physically crosslinked silk hydrogels can be prepared through sonication-induced sol-gel transition, negating any need for chemical crosslinking (Wang et al., 2008a).

In addition to providing a physical scaffold for cell growth and tissue formation, native extracellular matrix (ECM) also serves as a storage depot for growth factors, protecting them from degradation and controlling their spatio-temporal delivery (Benoit and Anseth, 2005; Wenk et al., 2010). Silk's ability to support cell, growth and proliferation has been extensively investigated (Acharya et al., 2008; Wang et al., 2006). Silk has also been shown to stabilize encapsulated proteins (Guziewicz et al., 2011; Lu et al., 2010; Lu et al., 2009) and exhibit retention and degradation-mediated release of incorporated growth factors (Wongpanit et al., 2010), suggesting silk also has the potential to sequester and locally deliver growth factors in a manner similar to the native ECM. In contrast to the collagen sponge BMP-2 carrier, silk biomaterials possess superior mechanical strength (Kluge et al., 2010) and tunable degradation and molecular weight (Wang et al., 2008a; Wray et al., 2011), reducing the risk of premature adsorption or compression.

Various silk materials, both alone and in combination with stem cells, have been investigated for bone regeneration *in vitro* and *in vivo* (Kundu and Kundu, 2010; Wang et al., 2006). Notably, Fini *et al.* found that silk hydrogels prepared through the addition of citric acid to a 2% (w/v) aqueous silk solution permitted the healing of confined critical size cancellous bone defects in rabbits and, compared with synthetic polymer control gels, greatly improved bone remodeling and maturation (Fini et al., 2005). Various silk material formats have also been investigated for BMP-2 delivery, including porous 3D sponges (Kirker-Head et al., 2007), films (Karageorgiou et al., 2004), microparticles (Bessa et al., 2010a; Bessa et al., 2010b; Wang et al., 2009), and electrospun mats (Li et al., 2006). Silk scaffolds seeded with genetically modified BMP-2 expressing cells have also been investigated (Jiang et al., 2009; Meinel et al., 2006).

The objective of this study was to use a critically-sized rat femoral segmental defect model to investigate the efficacy of a delivery system consisting of an electrospun polycaprolactone (PCL) nanofiber mesh tube with a silk hydrogel for local BMP-2 delivery

Materials and Methods

Preparation of silk hydrogels with and without BMP-2

Silk fibroin solution was prepared as previously described (Sofia et al., 2001). Briefly, cocoons of *B. mori* silkworm silk (Tajima Shoji Co.) were boiled for 30 minutes in a solution of 0.02 M Na_2CO_3 and rinsed, then dried at ambient conditions overnight. The dried fibroin was solubilized in a 9.3 M aqueous LiBr solution at 60°C for 4 hours, yielding a 20% (w/v) solution. LiBr was then removed from the solution by dialyzing the solution against distilled water for 2.5 days using Slide-a-Lyzer dialysis cassettes (MWCO 3,500, Pierce). Silk fibroin concentration was determined by evaporating water from a solution sample of known volume and massing using an analytical balance. Silk solutions were stored at 4–7°C before use. Silk solution was sterile filtered through a 0.22 μm membrane.

Silk hydrogels were formed using the sonication-induced gelation process previously described (Wang et al., 2008a). Prior to the onset of gelation, the silk solution was mixed with BMP-2 solution to a final concentration (w/v) of 1% or 2% at room temperature. BMP-2 solution was prepared by the reconstitution of rhBMP-2 (R&D Systems) according to the manufacturer instructions.

Silk hydrogel BMP-2 release

Bulk loaded silk hydrogels at a concentration (w/v) of 1% or 2% (2 groups; n = 3 per group) were aliquoted into LoBind low-protein-binding 1.5 mL Eppendorf tubes (150 μL total volume per gel, 3 μg BMP-2 loaded per gel). 0.5 mL of PBS was added to each hydrogel sample and samples were incubated at 37°C. Every 24 hours for 4 days, the buffer solution was removed and replaced with fresh PBS. The removed PBS was assayed for BMP-2 content using ELISA R&D Systems).

Animals and surgical procedure

An established, critically-sized, rat femoral segmental defect model was used in this study (Boerckel et al., 2011; Dupont et al., 2011; Kolambkar et al., 2011b; Oest et al., 2007). Bilateral 8 mm segmental femoral defects were created in 15 13-week-old SASCO Sprague Dawley rats. Prior to creating the defects, the femurs were stabilized using a custom modular fixation plate that allows longitudinal assessment of bone regeneration using X-ray radiography and microcomputed topography (μCT). The defects were divided into 4 groups (1% Silk, n = 5; 2% Silk, n = 5; 1% Silk + BMP-2, n =10; 2% Silk + BMP-2, n =10). An empty defect group was not included because we have previously shown that 8 mm segmental femoral defects do not heal if left empty (Oest et al., 2007). Electrospun PCL nanofiber mesh tubes with uniformly distributed 1 mm diameter perforations were fitted onto the bone defect ends such that the lumen of the tubes contained the defect (Kolambkar et al., 2011b) (Figs. 1a and 1b). The fabrication of the PCL nanofiber mesh tubes is described elsewhere (Kolambkar et al., 2011b). A volume of 200 μl of pre-gelled silk with or without 5 μg of BMP-2 was injected into each defect using a 22 gauge needle (Fig. 1b). All animals were housed under standard laboratory conditions and had free access to food and water. Due to post-surgery complications, 3 rats were removed from the study at different time points (two rats after 1 week of surgery; one rat after 4 weeks of surgery). One rat had a complication on the left limb developed 3 weeks after surgery. Data obtained from that limb were excluded from the analyses. One of the rats had to be sacrificed following weeks of surgery because of a dislocated plate. All the remaining animals were sacrificed 12 weeks after surgery. Following sacrifice, the extracted femurs were either subjected to biomechanical testing or assigned for histology. All procedures were approved by the Institutional Animal Care and Use Committee at the Georgia Institute of Technology.

X-ray radiography and μCT imaging

Bone regeneration was longitudinally assessed using 2D X-ray radiography (Faxitron MX-20 Digital, Faxitron X-ray Corp) and 3D μCT imaging (Viva-CT, Scanco Medical). For X-ray radiography, the femurs were imaged with an exposure time of 15 sec and voltage of 25 kW at 2, 4, 8, and 12 weeks post surgery. From the X-ray radiographs, bone bridging rate was qualitatively assessed by two independent investigators blinded to the treatment group. The femurs were also subjected to μCT imaging. The femurs were imaged at 38.5 μm resolution, 55 kVp voltage and 109 μA. Bone volume and bone mineral density were analyzed (σ = 1.2, support = 1, global threshold = 386 mg hydroxylapatite/cm^3) in 120 slices (4.56 mm) located in the center of the defect region.

Biomechanical testing

To assess functional restoration of the injured limbs, the extracted femurs were subjected to torsional loading (3°/sec) on a Bose ElectroForce system (ELF 3200, Bose EnduraTEC). The ends of the extracted femurs were cleaned from soft tissues and embedded in wood's metal (Alfa Aesar) for testing. Mechanical properties investigated included torsional stiffness and maximum torque. The torsional stiffness was calculated from the slope of the linear region of the torque-rotation data.

Histology

One representative sample from each group was designated for histology. The samples were placed in 10% neutral buffered formalin for 2 days and then decalcified for 2 weeks using a formic acid-based decalcifier (Cal-ExII, Fisher Scientific) (Boerckel et al., 2011). Following dehydration through a graded series of ethanols (70–100%), the samples were infiltrated and embedded in paraffin. Mid-saggital sections were cut at 4 μm thick using a microtome (HM 355S, MICROM) and stained with hematoxylin and eosin (H&E).

Statistical analysis

In vitro BMP-2 release from the 1% and 2% silk hydrogels was compared using student's t-tests. Bridging rates were compared using Pearson Chi-Square tests followed by Fisher's exact tests. Following a normality check, differences in bone volume, bone mineral density, torsional stiffness, and maximum torque among the four groups (1% Silk, 2% Silk, 1% Silk + BMP-2, 2% Silk + BMP-2) were examined using one-way analysis of variance (ANOVA) tests with Fisher's protected least-significant difference (PLSD) post-hoc tests. For those variables failing the normality test, Kruskal–Wallis tests were used. When the Kruskal–Wallis test revealed a significant difference ($p<0.05$), it was followed by a Mann-Whitney test.

After combining the 1% Silk group with the 2% Silk group, and the 1% Silk + BMP-2 group with the 2% Silk + BMP-2 group, differences in bone volume, bone mineral density, torsional stiffness, and maximum torque were compared using student's t-tests for the variables with a normal distribution. A Mann-Whitney test was used for the variables violating the normality assumption.

For all tests, a value of $p < 0.05$ was considered statistically significant. MINITAB 15 (Minitab, Inc.) was used for all the statistical analyses.

Results

Both the 1% and 2% silk hydrogels exhibited burst release of BMP-2 (approx. 70–90% of the cumulative release within the first 24 hours) (Fig. 2). The 1% and 2% silk hydrogels released approx. 40% (1.21 μg) and approx. 22% (0.67 μg) of their total BMP-2 load, respectively. Though they were prepared with the same initial total BMP-2 load per hydrogel, the 1% silk hydrogels released nearly twice as much BMP-2 as 2% silk hydrogels during the 4 day time frame tested. The 1% silk hydrogels released significantly more BMP-2 within the first 24 hours than the 2% silk hydrogels ($p < 0.05$).

Despite the differences in *in vitro* BMP-2 release kinetics, none of the outcomes of the animal study revealed significant differences between the 1% Silk + BMP-2 and 2% Silk +BMP-2 groups. Also, no significant differences in any of the outcomes of the animal study were found between the 1% Silk and 2% Silk groups. The 1% Silk + BMP-2 group had greater bone volume than the 1% Silk group at 8 and 12 weeks ($p < 0.05$; Fig. 3). Compared to the 2% Silk group, the 2% Silk + BMP-2 group had a higher bridging rate and more bone

volume at 4, 8, and 12 weeks ($p < 0.05$; Table 1; Fig. 3). No significant differences in BMD or the biomechanical properties were found (Table 2; Fig. 4).

As no effects of silk concentration were found, both concentrations of silk were combined (i.e. 1% Silk and 2% Silk groups were combined in one group: Silk; 1% Silk + BMP-2 and 2% Silk + BMP-2 groups were combined in one group: Silk + BMP-2). After combining the groups, it was found that the Silk + BMP-2 group formed more bone than the Silk group at 4, 8, and 12 weeks (Figs. 5 and 6). The addition of BMP-2 to silk also resulted in a significant improvement in the biomechanical properties. The torsional stiffness and maximum torque in the Silk + BMP-2 group were greater than 50- and 10-fold higher, respectively, compared to the Silk group (Fig. 7). No significant differences in BMD were found at any of the examined time points. Histological examination of the defect region showed that normal bone tissue formed in the Silk + BMP-2 group, while fibrous-like tissue filled the defect region in the Silk group (Fig. 8). No residuals of the silk hydrogel in the defect region were found in either group, indicating that the silk hydrogel have been completely degraded by 12 weeks.

Discussion

The results reported here show that silk is an effective carrier for BMP-2. Compared to the delivery system without BMP-2, the delivery system that contained BMP-2 resulted in more bone formation at 4, 8, 12 weeks after treatment. Importantly, the biomechanical properties were also improved in the presence of BMP-2, indicating functional repair of the defect region. These findings are consistent with a recent study that demonstrated, in a rabbit sinus defect model, the effectiveness of a silk hydrogel carrier of BMP-2 to repair bone defects (Zheng et al., 2011). To the best of our knowledge, this is the first investigation to examine the effects of delivering BMP-2 in a silk hydrogel on functional repair of critically-sized long bone defects.

It has been previously shown that that a delivery system consisting of an electrospun nanofiber mesh tube and BMP-2 mixed with RGD (Arg-Gly-Asp sequence) functionalized alginate (RGD-alginate) promotes significantly better segmental bone defect healing than the clinical standard of BMP-2 delivery on a collagen sponge (Boerckel et al., 2011; Kolambkar et al., 2011a). Boerckel et al [2011] have found that following 12 weeks of treatment with an electrospun nanofiber mesh tube and 5ug of BMP-2 mixed with RGD-alginate the bridging rate was 100% and the regenerated bone volume was 92 ± 5 [mm^3]. The values of torsional stiffness and maximum torque were 0.050 ± 0.015 [N-m/Deg] and 0.18 ± 0.03 [N-m], respectively (Boerckel et al., 2011). In this study, we used the same delivery system, but silk was used instead of RGD-alginate. Although the biomechanical properties were comparable (Fig. 7), the bridging rate and bone volume values in our study were lower compared to those reported by Boerckel et al [2011] (Table 1; Fig. 6c). It would be expected that the difference in bone volume between the two studies will translate to substantial differences in the biomechanical properties; however, that was not the case. This could be explained by considering the differences in the degradation rates between the RGD-alginate used in Boerckel et al [2011] and the silk used in this study. Histological analyses showed that fragments of the alginate hydrogel are clearly visible in the defect region following 12 weeks of treatment, indicating that the RGD-alginate did not fully degrade (Boerckel et al., 2011). In this investigation, no residuals of the silk in the defect region were found. The presence of a hydrogel could impede the biomechanical properties by preventing complete bone interconnectivity (Boerckel et al., 2011). Furthermore, complete degradation of the hydrogel during the regeneration phase of bone defect healing may facilitate subsequent remodeling and restoration of normal diaphyseal morphology.

Future studies are still needed to determine the mechanistic basis of the differences in bone volume between the two studies.

It is also important to note that the intact bone biomechanical properties of femurs obtained from age-matched rats are 0.030 ± 0.001 N-m/deg and 0.31 ± 0.02 N-m for torsional stiffness and maximum torque, respectively (Kolambkar et al., 2011b). These values are only slightly higher than the values obtained from the group treated with Silk + BMP-2 (Fig. 7). If we exclude the specimens that did not bridge from the analyses, torsional stiffness and maximum torque of the Silk + BMP-2 group were 17% and 13%, respectively, higher than those of intact bone. This suggests that for the defects that bridged, the regenerated bone was interconnected and integrated well with the native bone.

We found differences in the *in vitro* release kinetics of BMP-2 between 1% and 2% silk hydrogels. The 1% silk released almost twice as much BMP-2 as the 2% silk during the first 4 days (Fig. 2). However, no statistically significant differences in the animal study were observed between the 1% Silk + BMP-2 and 2% Silk + BMP-2 groups. This may suggest that the magnitude of the differences in the BMP-2 release kinetics between the two silk concentrations is not enough to result in substantial differences *in vivo*. An alternative explanation could be that in the presence of an osteoinductive factor such as BMP-2 there is an effect of silk concentration itself on bone regeneration that has masked the effect of the difference in BMP-2 release. For example, it may be that BMP-2 release profile from the 2% silk is more advantageous than BMP-2 release profile from the 1% silk, but the 1% silk degradation properties are better for bone regeneration than the 2% silk. Investigating the degradation properties of different silk concentrations at early time points could provide an insight on why no significant differences between the 1% Silk + BMP-2 and 2% Silk + BMP-2 groups were found.

The results reported here should be interpreted with several limitations in mind. Although *in vivo* BMP-2 release kinetics have been previously assessed by tagging BMP-2 to an *in vivo* NIR fluorochrome label (Boerckel et al., 2011), no attempt has been made to investigate the differences in BMP-2 release profile between the 1% and 2% silk hydrogels *in vivo*, which could vary significantly from *in vitro* release behavior due to degradation of the silk hydrogel. Also, because we had a number of animal complications during the course of the study, the statistical power of this preliminary investigation was reduced.

In conclusion, using a critically-sized, rat femoral segmental defect model, we have shown that a BMP-2 delivery system consisting of an electrospun PCL nanofiber mesh tube with a silk hydrogel represents an effective strategy for functional repair of large bone defects. The findings of this work provide new insight into the use of silk hydrogel as a growth factor carrier.

Acknowledgments

This research study was supported by NIH grants EB003210, EB002520, and AR056694 and the Armed Forces Institute for Regenerative Medicine. The authors would like to thank Sha'Aqua Asberry and Hazel Stevens for assistance in the histological analysis. We would like to thank the following individuals for their help in surgeries: Christopher Dosier, Angela Lin, Dr Nick Willett, Hazel Stevens, Jason Wang, Alice Li, Ashley Allen. We would like to thank David Reece for help with the μCT imaging analysis.

Funding sources:

NIH grants EB003210, EB002520, and AR056694

Armed Forces Institute for Regenerative Medicine.

References

Acharya C, Ghosh SK, Kundu SC. Silk fibroin protein from mulberry and non-mulberry silkworms: cytotoxicity, biocompatibility and kinetics of L929 murine fibroblast adhesion. J Mater Sci Mater Med. 2008; 19:2827–2836. [PubMed: 18322779]

Benoit DS, Anseth KS. Heparin functionalized PEG gels that modulate protein adsorption for hMSC adhesion and differentiation. Acta Biomater. 2005; 1:461–470. [PubMed: 16701827]

Bessa PC, Balmayor ER, Azevedo HS, Nurnberger S, Casal M, van Griensven M, Reis RL, Redl H. Silk fibroin microparticles as carriers for delivery of human recombinant BMPs. Physical characterization and drug release. J Tissue Eng Regen Med. 2010a; 4:349–355. [PubMed: 20058243]

Bessa PC, Balmayor ER, Hartinger J, Zanoni G, Dopler D, Meinl A, Banerjee A, Casal M, Redl H, Reis RL, van Griensven M. Silk fibroin microparticles as carriers for delivery of human recombinant bone morphogenetic protein-2: in vitro and in vivo bioactivity. Tissue Eng Part C Methods. 2010b; 16:937–945. [PubMed: 19958078]

Boerckel JD, Kolambkar YM, Dupont KM, Uhrig BA, Phelps EA, Stevens HY, Garcia AJ, Guldberg RE. Effects of protein dose and delivery system on BMP-mediated bone regeneration. Biomaterials. 2011; 32:5241–5251. [PubMed: 21507479]

Carragee EJ, Hurwitz EL, Weiner BK. A critical review of recombinant human bone morphogenetic protein-2 trials in spinal surgery: emerging safety concerns and lessons learned. Spine J. 2011; 11:471–491. [PubMed: 21729796]

Chen B, Lin H, Wang J, Zhao Y, Wang B, Zhao W, Sun W, Dai J. Homogeneous osteogenesis and bone regeneration by demineralized bone matrix loading with collagen-targeting bone morphogenetic protein-2. Biomaterials. 2007; 28:1027–1035. [PubMed: 17095085]

Dupont KM, Boerckel JD, Stevens HY, Diab T, Kolambkar YM, Takahata M, Schwarz EM, Guldberg RE. Synthetic scaffold coating with adeno-associated virus encoding BMP2 to promote endogenous bone repair. Cell Tissue Res. 2011

Fini M, Motta A, Torricelli P, Giavaresi G, Nicoli Aldini N, Tschon M, Giardino R, Migliaresi C. The healing of confined critical size cancellous defects in the presence of silk fibroin hydrogel. Biomaterials. 2005; 26:3527–3536. [PubMed: 15621243]

Glassman SD, Carreon L, Djurasovic M, Campbell MJ, Puno RM, Johnson JR, Dimar JR. Posterolateral lumbar spine fusion with INFUSE bone graft. Spine J. 2007; 7:44–49. [PubMed: 17197332]

Guziewicz N, Best A, Perez-Ramirez B, Kaplan DL. Lyophilized silk fibroin hydrogels for the sustained local delivery of therapeutic monoclonal antibodies. Biomaterials. 2011; 32:2642–2650. [PubMed: 21216004]

Horan RL, Antle K, Collette AL, Wang Y, Huang J, Moreau JE, Volloch V, Kaplan DL, Altman GH. In vitro degradation of silk fibroin. Biomaterials. 2005; 26:3385–3393. [PubMed: 15621227]

Jiang X, Zhao J, Wang S, Sun X, Zhang X, Chen J, Kaplan DL, Zhang Z. Mandibular repair in rats with premineralized silk scaffolds and BMP-2-modified bMSCs. Biomaterials. 2009; 30:4522–4532. [PubMed: 19501905]

Karageorgiou V, Meinel L, Hofmann S, Malhotra A, Volloch V, Kaplan D. Bone morphogenetic protein-2 decorated silk fibroin films induce osteogenic differentiation of human bone marrow stromal cells. J Biomed Mater Res A. 2004; 71:528–537. [PubMed: 15478212]

Kirker-Head C, Karageorgiou V, Hofmann S, Fajardo R, Betz O, Merkle HP, Hilbe M, von Rechenberg B, McCool J, Abrahamsen L, Nazarian A, Cory E, Curtis M, Kaplan D, Meinel L. BMP-silk composite matrices heal critically sized femoral defects. Bone. 2007; 41:247–255. [PubMed: 17553763]

Kluge JA, Rosiello NC, Leisk GG, Kaplan DL, Dorfmann AL. The consolidation behavior of silk hydrogels. J Mech Behav Biomed Mater. 2010; 3:278–289. [PubMed: 20142112]

Kolambkar YM, Boerckel JD, Dupont KM, Bajin M, Huebsch N, Mooney DJ, Hutmacher DW, Guldberg RE. Spatiotemporal delivery of bone morphogenetic protein enhances functional repair of segmental bone defects. Bone. 2011a; 49:485–492. [PubMed: 21621027]

Kolambkar YM, Dupont KM, Boerckel JD, Huebsch N, Mooney DJ, Hutmacher DW, Guldberg RE. An alginate-based hybrid system for growth factor delivery in the functional repair of large bone defects. Biomaterials. 2011b; 32:65–74. [PubMed: 20864165]

Kundu B, Kundu SC. Osteogenesis of human stem cells in silk biomaterial for regenerative therapy. Prog Polym Sci. 2010; 35:1116–1127.

Lawrence BD, Cronin-Golomb M, Georgakoudi I, Kaplan DL, Omenetto FG. Bioactive silk protein biomaterial systems for optical devices. Biomacromolecules. 2008; 9:1214–1220. [PubMed: 18370418]

Leal-Egana A, Scheibel T. Silk-based materials for biomedical applications. Biotechnol Appl Biochem. 2010; 55:155–167. [PubMed: 20222871]

Li C, Vepari C, Jin HJ, Kim HJ, Kaplan DL. Electrospun silk-BMP-2 scaffolds for bone tissue engineering. Biomaterials. 2006; 27:3115–3124. [PubMed: 16458961]

Lu Q, Wang X, Hu X, Cebe P, Omenetto F, Kaplan DL. Stabilization and release of enzymes from silk films. Macromol Biosci. 2010; 10:359–368. [PubMed: 20217856]

Lu S, Wang X, Lu Q, Hu X, Uppal N, Omenetto FG, Kaplan DL. Stabilization of enzymes in silk films. Biomacromolecules. 2009; 10:1032–1042. [PubMed: 19323497]

Luginbuehl V, Meinel L, Merkle HP, Gander B. Localized delivery of growth factors for bone repair. Eur J Pharm Biopharm. 2004; 58:197–208. [PubMed: 15296949]

Meinel L, Hofmann S, Betz O, Fajardo R, Merkle HP, Langer R, Evans CH, Vunjak-Novakovic G, Kaplan DL. Osteogenesis by human mesenchymal stem cells cultured on silk biomaterials: comparison of adenovirus mediated gene transfer and protein delivery of BMP-2. Biomaterials. 2006; 27:4993–5002. [PubMed: 16765437]

Meinel L, Hofmann S, Karageorgiou V, Kirker-Head C, McCool J, Gronowicz G, Zichner L, Langer R, Vunjak-Novakovic G, Kaplan DL. The inflammatory responses to silk films in vitro and in vivo. Biomaterials. 2005; 26:147–155. [PubMed: 15207461]

Numata K, Kaplan DL. Silk-based delivery systems of bioactive molecules. Adv Drug Deliv Rev. 2010; 62:1497–1508. [PubMed: 20298729]

Oest ME, Dupont KM, Kong HJ, Mooney DJ, Guldberg RE. Quantitative assessment of scaffold and growth factor-mediated repair of critically sized bone defects. J Orthop Res. 2007; 25:941–950. [PubMed: 17415756]

Panilaitis B, Altman GH, Chen J, Jin HJ, Karageorgiou V, Kaplan DL. Macrophage responses to silk. Biomaterials. 2003; 24:3079–3085. [PubMed: 12895580]

Seo YK, Yoon HH, Song KY, Kwon SY, Lee HS, Park YS, Park JK. Increase in cell migration and angiogenesis in a composite silk scaffold for tissue-engineered ligaments. J Orthop Res. 2009; 27:495–503. [PubMed: 18924141]

Sofia S, McCarthy MB, Gronowicz G, Kaplan DL. Functionalized silk-based biomaterials for bone formation. J Biomed Mater Res. 2001; 54:139–148. [PubMed: 11077413]

Suh DY, Boden SD, Louis-Ugbo J, Mayr M, Murakami H, Kim HS, Minamide A, Hutton WC. Delivery of recombinant human bone morphogenetic protein-2 using a compression-resistant matrix in posterolateral spine fusion in the rabbit and in the non-human primate. Spine (Phila Pa 1976). 2002; 27:353–360. [PubMed: 11840099]

Vepari C, Kaplan DL. Silk as a Biomaterial. Prog Polym Sci. 2007; 32:991–1007. [PubMed: 19543442]

Wang X, Kluge JA, Leisk GG, Kaplan DL. Sonication-induced gelation of silk fibroin for cell encapsulation. Biomaterials. 2008a; 29:1054–1064. [PubMed: 18031805]

Wang X, Wenk E, Zhang X, Meinel L, Vunjak-Novakovic G, Kaplan DL. Growth factor gradients via microsphere delivery in biopolymer scaffolds for osteochondral tissue engineering. J Control Release. 2009; 134:81–90. [PubMed: 19071168]

Wang Y, Kim HJ, Vunjak-Novakovic G, Kaplan DL. Stem cell-based tissue engineering with silk biomaterials. Biomaterials. 2006; 27:6064–6082. [PubMed: 16890988]

Wang Y, Rudym DD, Walsh A, Abrahamsen L, Kim HJ, Kim HS, Kirker-Head C, Kaplan DL. In vivo degradation of three-dimensional silk fibroin scaffolds. Biomaterials. 2008b; 29:3415–3428. [PubMed: 18502501]

Wenk E, Murphy AR, Kaplan DL, Meinel L, Merkle HP, Uebersax L. The use of sulfonated silk fibroin derivatives to control binding, delivery and potency of FGF-2 in tissue regeneration. Biomaterials. 2010; 31:1403–1413. [PubMed: 19942287]

Wongpanit P, Ueda H, Tabata Y, Rujiravanit R. In vitro and in vivo release of basic fibroblast growth factor using a silk fibroin scaffold as delivery carrier. J Biomater Sci Polym Ed. 2010; 21:1403–1419. [PubMed: 20534193]

Wray LS, Hu X, Gallego J, Georgakoudi I, Omenetto FG, Schmidt D, Kaplan DL. Effect of processing on silk-based biomaterials: Reproducibility and biocompatibility. J Biomed Mater Res B Appl Biomater. 2011

Zheng W, Wang S, Sun X, Zhang X, Chen J, Kaplan DL, Jiang X. Injectable sonication induced silk hydrogel for VEGF165 and BMP-2 delivery to elevate the maxillary sinus floor in rabbit. Biomaterials. 2011 In Press.

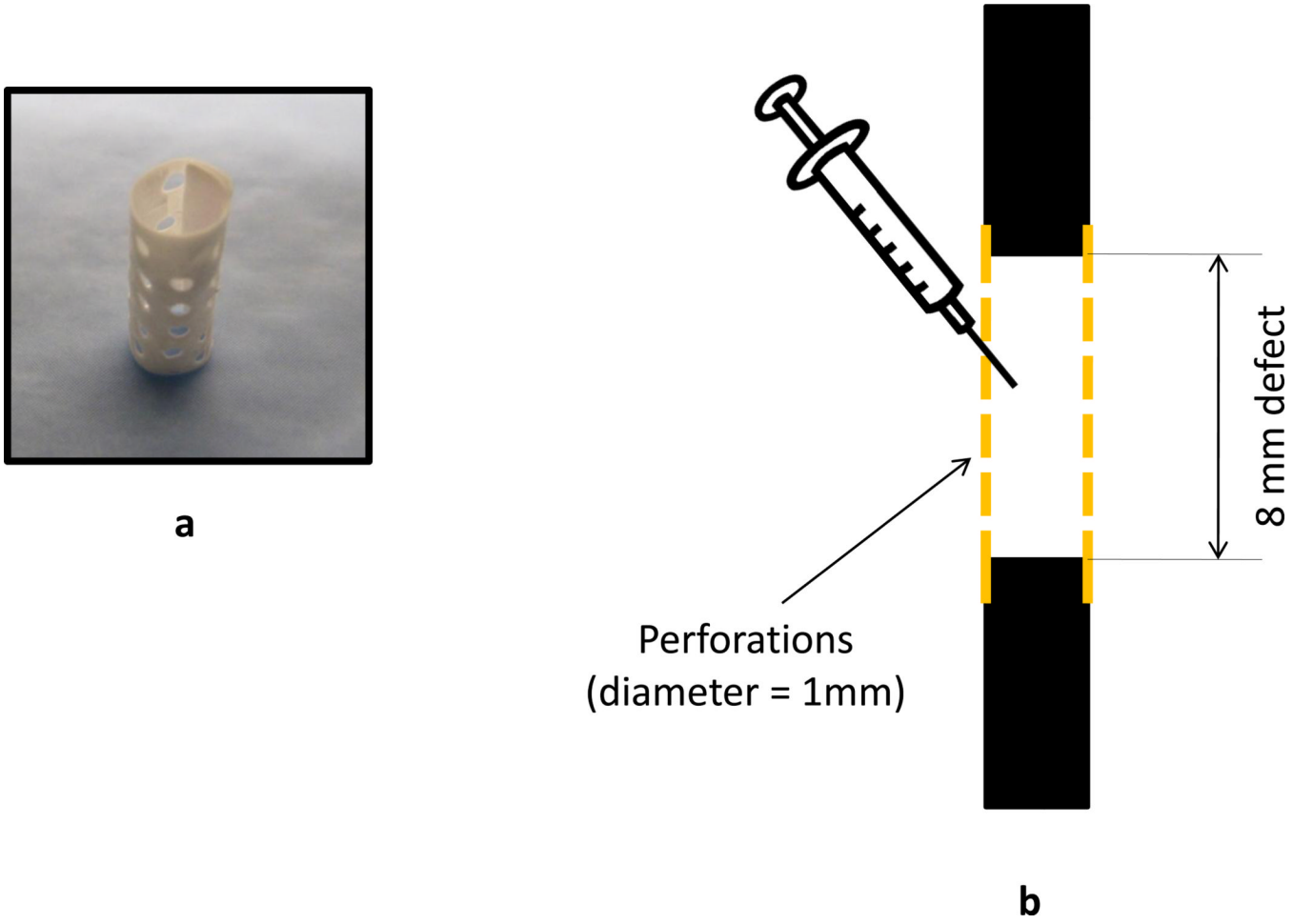

Figure 1.
a) Perforated electrospun PCL nanofiber mesh tube (inner diameter: 4.5 mm; height: 12 mm). b) Schematic of the defect region. Perforated electrospun PCL nanofiber mesh tube is placed around the defect. Pregelled silk hydrogel with or without BMP-2 is injected into the defect.

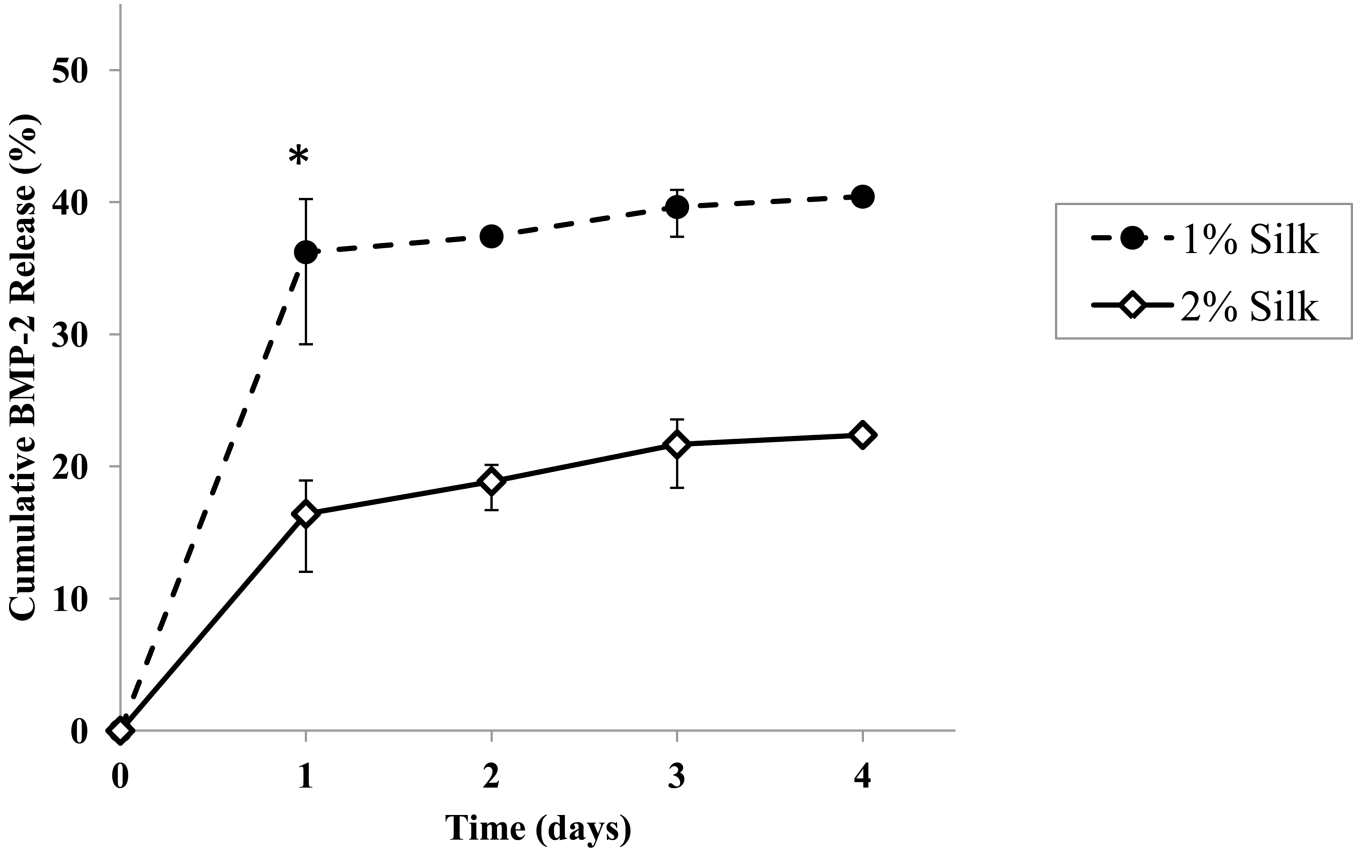

Figure 2.
Cumulative release of BMP-2 from 1% and 2% BMP-2 bulk-loaded silk hydrogels. n=3/group. Data presented as ± SE mean (where error bars are not shown they fall into background). *: significant difference in the amount of BMP-2 released at day 1.

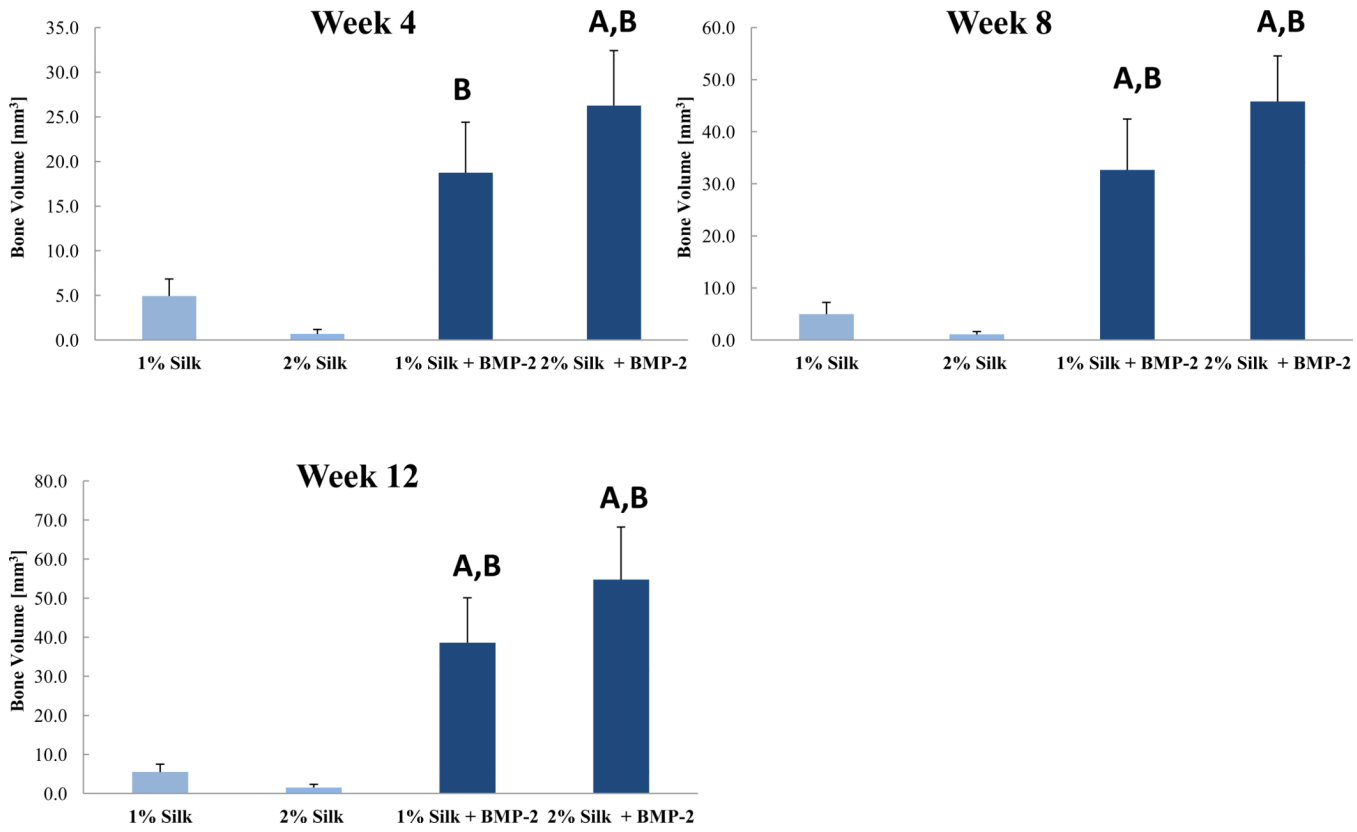

Figure 3.

Regenerated bone volume at the 4-, 8-, and 12-week time points. Week 4: n = 5 for the 1% Silk group, n = 5 for the 2% Silk group, n = 8 for the 1% Silk + BMP-2 group, n = 6 for the 2% Silk + BMP-2 group. Week 8: n = 5 for the 1% Silk group, n = 4 for the 2% Silk group, n = 7 for the 1% Silk + BMP-2 group, n = 6 for the 2% Silk + BMP-2 group. Week 12: n = 5 for the 1% Silk group, n = 4 for the 2% Silk group, n = 7 for the 1% Silk + BMP-2 group, n = 5 for the 2% Silk + BMP-2 group. Data are presented as +SE mean. A: Significantly different than 1% Silk; B: Significantly different than 2% Silk.

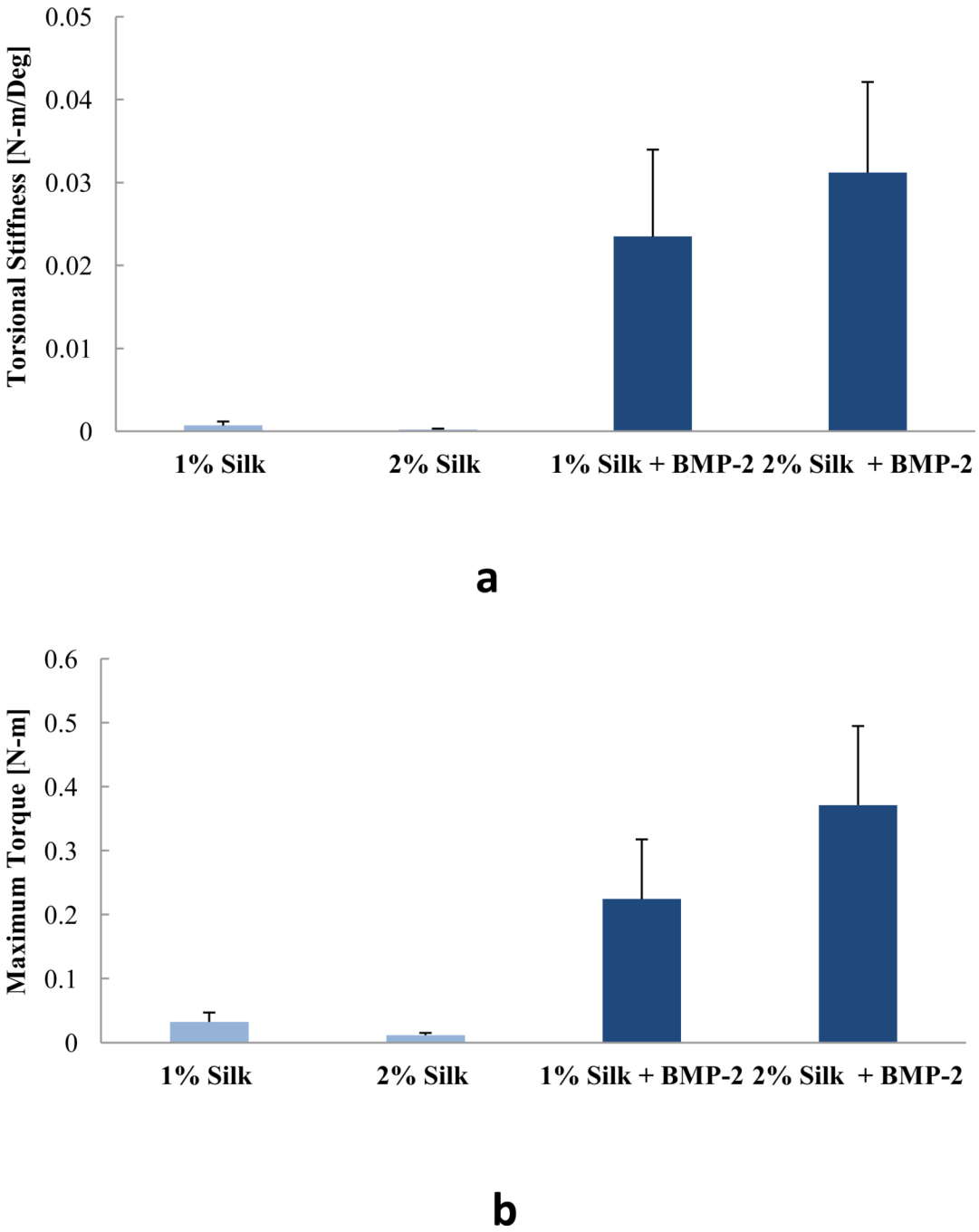

Figure 4.
Biomechanical properties of the extracted femurs. a) Torsional stiffness. b) Maximum torque. n = 5 for the 1% Silk group, n = 4 for the 2% Silk group, n = 7 for the 1% Silk + BMP-2 group, n = 5 for the 2% Silk + BMP-2 group. Data are presented as +SE mean.

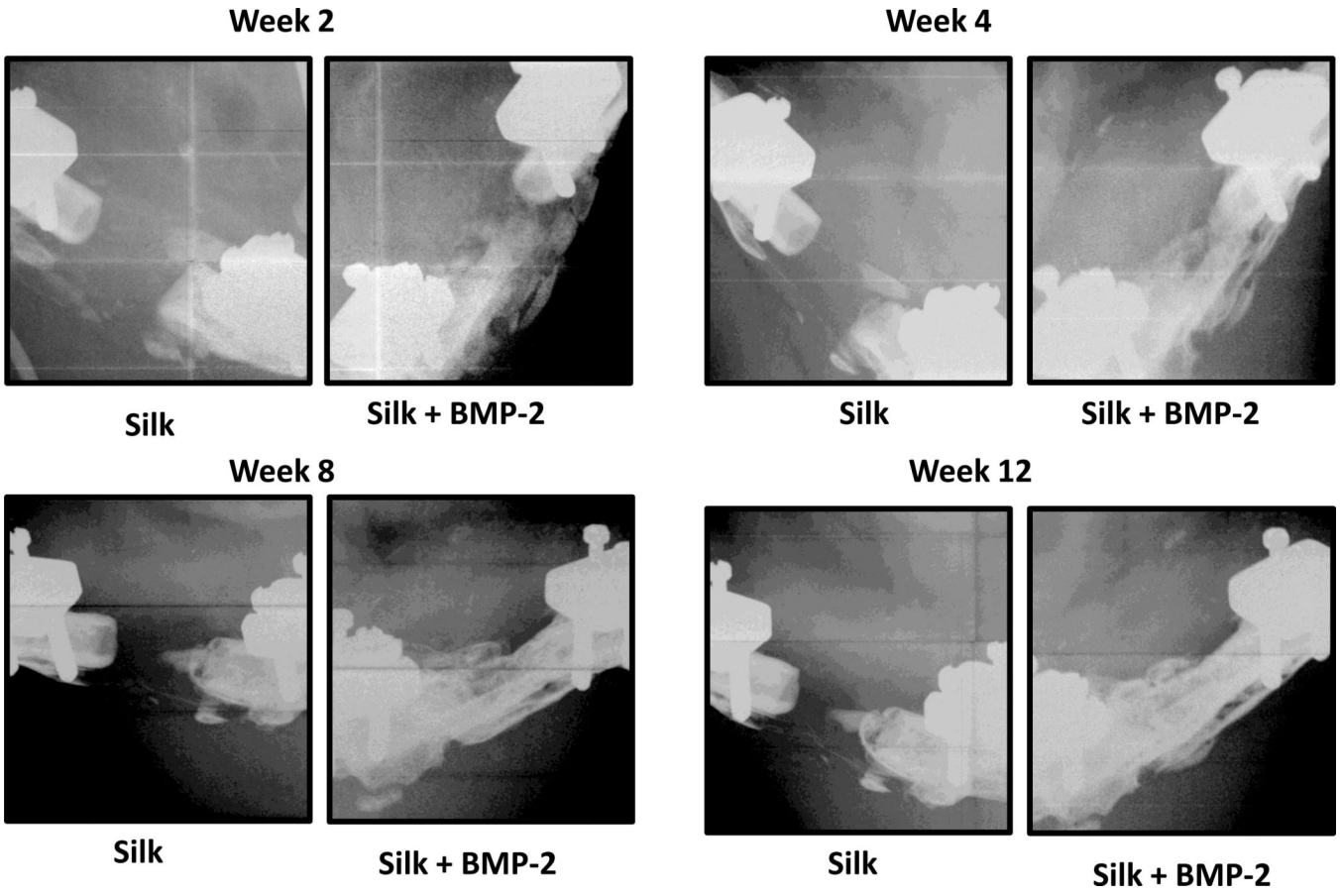

Figure 5.
Representative X-ray radiography images obtained at the 4-, 8-, and 12-week time points.

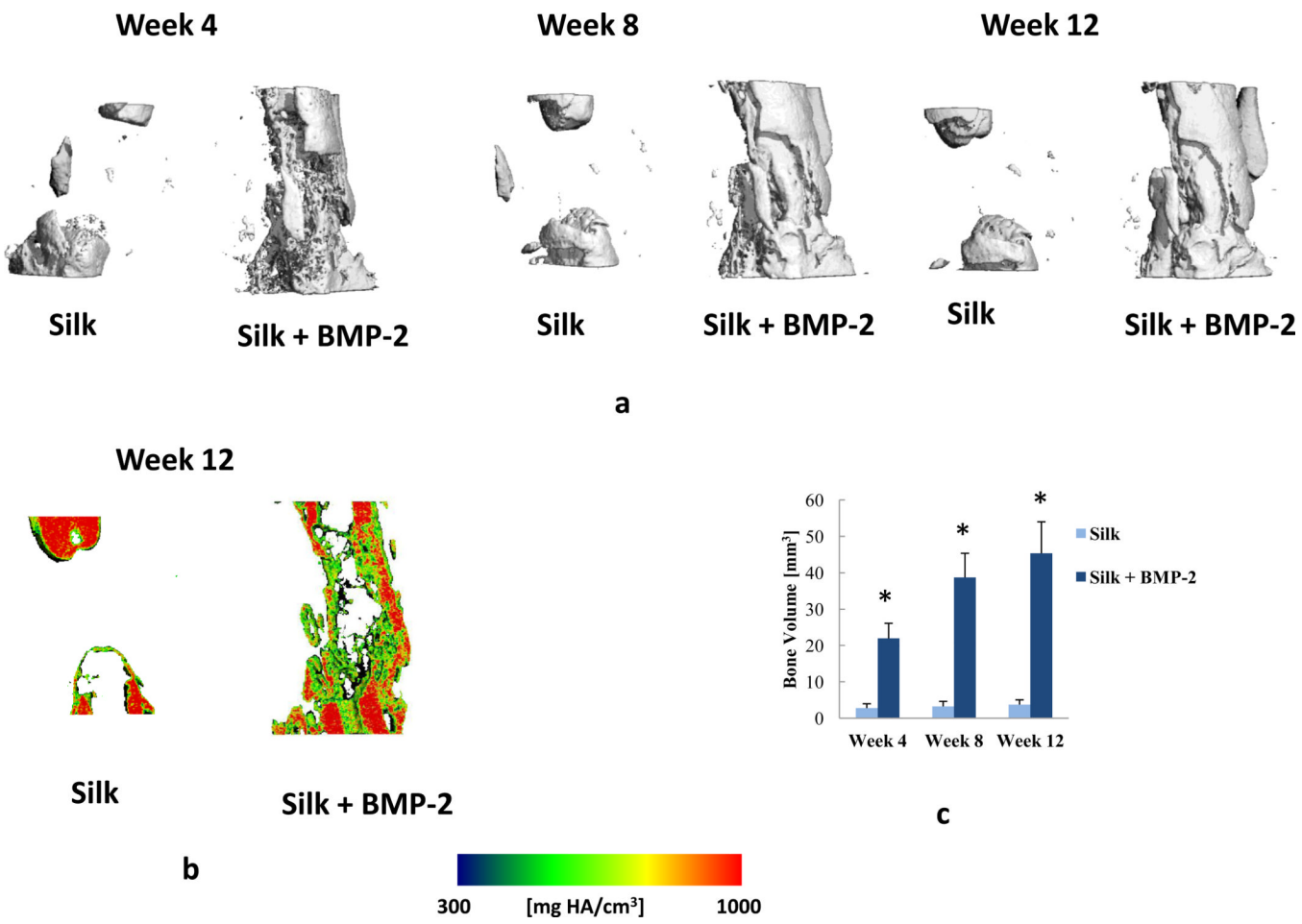

Figure 6.

a) Representative μCT images obtained at the 4-, 8-, and 12-week time points. b) μCT images obtained at the 12-week time point showing sagittal cross sections with local mineral density maps. c) Regenerated bone volume after combining the groups at the 4-, 8-, and 12-week time points. Week 4: n = 10 for the silk group, n = 14 for the silk + BMP-2 group. Week 8: n = 9 for the silk group, n = 13 for the silk + BMP-2 group. Week 12: n = 9 for the silk group, n = 12 for the silk + BMP-2 group. Data are presented as +SE mean. *: significant difference between the Silk and Silk +BMP-2 groups at the same time point.

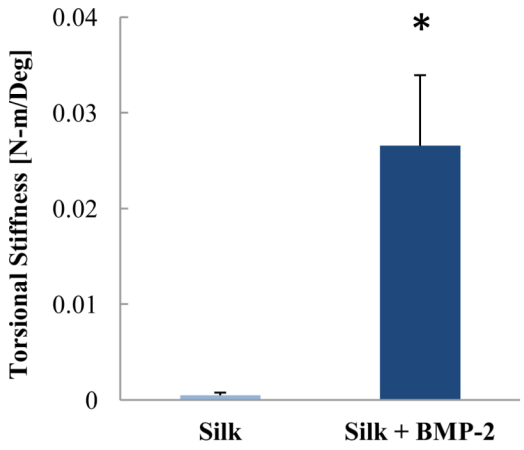

a

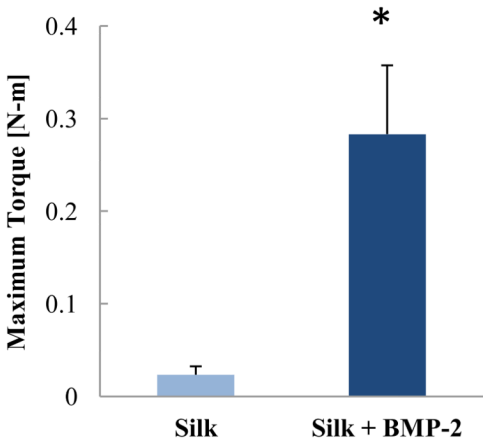

b

Figure 7.

Biomechanical properties of the extracted femurs after combining the groups. a) Torsional stiffness. b) Maximum torque. n = 7 for the silk group, n = 10 for the silk + BMP-2 group. Data are presented as +SE mean. *: significant difference.

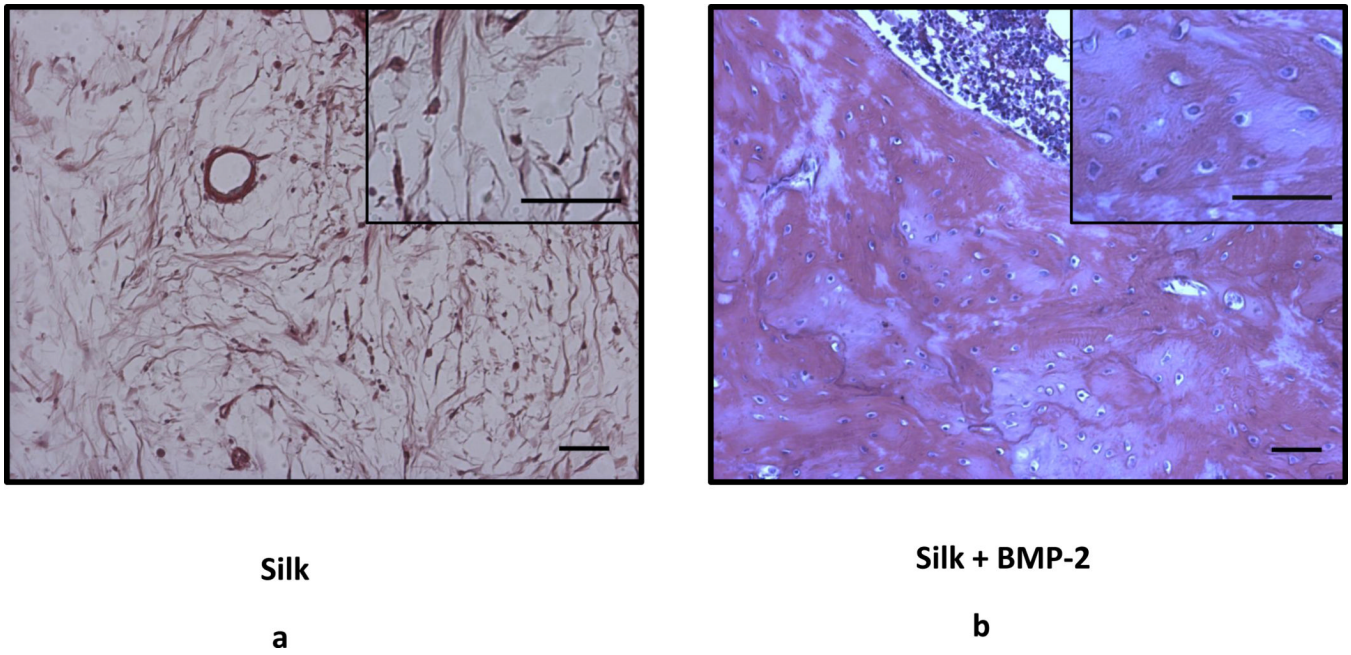

Figure 8.
Images from H&E stained sections. Scale bar: 50 μm.

Table 1

Bridging rates at the 2-, 4-, 8-, and 12-week time points. A: Significantly different than 1% Silk; B: Significantly different than 2% Silk.

	1% Silk	2% Silk	1% Silk + BMP-2	2% Silk + BMP-2	*p* value
Week 2	0/5	0/5	0/8	0/6	N/A
Week 4	0/5	0/5	3/8	4/6	< 0.05
Week 8	0/5	0/4	4/7	5/6[A,B]	< 0.05
Week 12	0/5	0/4	4/7	4/5[A,B]	< 0.05

Table 2

Regenerated bone mineral density at the 4-, 8-, and 12-week time points.

	1% Silk		2% Silk		1% Silk + BMP-2		2% Silk + BMP-2		*p* value
Week 4	528.3	180.5	690.9	23.0	679.5	14.6	658.2	15.2	p = 0.820
Week 8	613.1	200.2	761.6	64.2	801.3	16.7	758.4	7.6	p = 0.397
Week 12	660.8	212.8	750.1	75.4	852.4	18.7	819.7	13.4	p = 0.509